MATERIALS CHEMISTRY FRONTIERS

CHINESE CHEMICAL SOCIETY

ROYAL SOCIETY OF CHEMISTRY

RESEARCH ARTICLE

View Article Online
View Journal | View Issue

Open Access Article. Published on 08 July 2022. Downloaded on 1/13/2026 10:55:49 PM.
This article is licensed under a Creative Commons Attribution 3.0 Unported Licence.

Check for updates

Cite this: *Mater. Chem. Front.*, 2022, **6**, 2491

Naphthaldehyde-based Schiff base dyes: aggregation-induced emission and high-contrast reversible mechanochromic luminescence†

Lingyi Shen,‡[a] Chang-Jin Yu,‡[a] Hai-Fang Xie,[a] Na Xu,[a] Hong Xu,[a] Ya-Li Huang,[a] Carl Redshaw,*[b] Xing Feng*[c] and Qi-Long Zhang*[a]

Received 7th June 2022,
Accepted 7th July 2022

DOI: 10.1039/d2qm00542e

rsc.li/frontiers-materials

Mechanochromic luminescent materials have attracted intense attention because of their excellent reversible optical behaviour, but the mechanism of the stimuli responsive behaviour remains ambiguous. Herein, a novel naphthaldehyde-based Schiff base, namely N^2,N^6-bis(2-(2-hydroxynaphthalen-1-yl)phenyl)pyridine-2,6-dicarboxamide (**HNP**) exhibiting both aggregation enhanced emission (AIEE) and excited state intramolecular proton transfer (ESIPT) characteristics has been synthesized. The mechanism of the reversible mechanochromism was investigated *via* experimental and theoretical procedures. Crystalline **HNP** exhibits a reversible mechanochromism from yellow to orange emission under external stimulus and back to yellow emission by fuming under a dichloromethane atmosphere. Single crystal X-ray diffraction analysis indicated that the compound **HNP** adopts two types of molecular conformations with different intramolecular torsion angles. Meanwhile, DFT and TD-DFT calculations demonstrated that the torsion angle change directly affects the electronic distribution, resulting in a discriminable energy gap. Clearly, the different molecular conformations play a crucial role in triggering the reversible mechanochromism upon grinding. Additionally, **HNP** is an excellent fluorescent probe for detecting Cu(II) ions in solution. Thus, this example not only provides clear evidence to clarify the mechanism of reversible mechanochromism, but also offers a new on-off chemosensor for Cu(II) ion detection.

1. Introduction

Mechanochromic luminescent (MCL) materials are a classical type of multifunctional material that can change emission colour reversibly under external stimulus, and these materials exhibit high efficiency toward diverse applications in sensors,[1] information anti-counterfeiting,[2] memory chips and optoelectronic devices.[3] Organic materials with mechanochromic luminescence properties show unique advantages[4] such as low cost, precise molecular structures with tunable optical properties. Moreover, molecular components with a twisted conformation have been utilized for constructing MCL materials, such as tetraphenylethylene,[5] cyanostyrene,[6] carbazole,[7] *etc.*

Aggregation-induced emission (AIE), is an abnormal fluorescence phenomenon, where a type of molecule is weakly fluorescent in solution but exhibits high fluorescence in the aggregated state.[8] Organic luminescent materials with the AIE characteristic have shown great potential in organic light-emitting diodes,[9] photodynamic therapy,[10] fluorescent probes,[11] *etc.* Excited-state intramolecular proton transfer (ESIPT) is a classical fluorescence process, where the proton can transfer from a hydrogen bond donor (*e.g.* –OH and –NH_2) to a hydrogen bond receptor (*e.g.* = N– and C═O)[12] *via* a tautomeric transformation under irradiation, resulting in a large red-shifted emission. Specifically, the combination of the AIE and ESIPT features can be used to overcome environmental sensitivity to avoid self-absorption.[13]

Schiff base compounds have wide versatility and exhibit good solubility in common solvents, in addition to being easily functionalized when needed for various applications. Previously, our group reported that the tetraphenylethylene functionalized

[a] *Research Center for Molecular Medical Engineering, School of Basic Medical Science, Guizhou Medical University, Guiyang 550004, China. E-mail: gzuqlzhang@126.com*
[b] *Department of Chemistry, University of Hull, Cottingham Road, Hull, Yorkshire HU6 7RX, UK. E-mail: c.redshaw@hull.ac.uk*
[c] *Guangdong Provincial Key Laboratory of Functional Soft Condensed Matter, School of Material and Energy, Guangdong University of Technology, Guangzhou 510006, P. R. China. E-mail: hyxhn@sina.com*

† Electronic supplementary information (ESI) available: Detailed experimental description, characterization and physical measurements (PDF). X-ray crystallographic data for the three compounds (CIF). CCDC 2174338–2174340. For ESI and crystallographic data in CIF or other electronic format see DOI: https://doi.org/10.1039/d2qm00542e

‡ L. Shen and C.-J. Yu contributed equally to this work.

Open Access Article. Published on 08 July 2022. Downloaded on 1/13/2026 10:55:49 PM.
This article is licensed under a Creative Commons Attribution 3.0 Unported Licence.

salicylaldehyde Schiff-base with the aggregation-induced enhanced emission (AIEE) property is an excellent fluorescent probe for Cu(II) ion detection[14] and we note that a naphthyl-based Schiff base zinc complex has been used for cellular uptake studies.[15] Moreover, the coordination mode of a salicylaldehyde Schiff-base fluorescent probe toward Cu(II) was evaluated by single crystal X-ray diffraction.[16] In recent years, many Schiff base MCL compounds have been reported[17] and proved to be excellent fluorescence carriers with high-contrast reversible mechanochromic luminescence properties.[18] Generally, photoluminescence spectra, scan/transmission electron microscopy, and powder X-ray-diffraction are the typical techniques employed for understanding the mechanochromic mechanism. However, understanding the intrinsic mechanism of MCL behaviour remains an enormous challenge.

In this work, a Schiff base compound **HNP** was synthesized *via* a facile one-step synthetic method, which exhibits typical AIEE plus ESIPT characteristics. Due to the presence of the flexible Schiff base skeleton, the AIEE-active molecule **HNP** adopts a twisted molecular conformation *via* several strong intra/inter-molecular interactions, which leads to different emissions in the crystalline state. More interestingly, this crystal displays high-contrast reversible mechanochromic luminescence properties *via* orange and yellow emission, and this result is ascribed to the different molecular conformations in the crystal packing. The relationship between the molecular packing and the emission properties is discussed to understand in greater depth the reversible mechanochromic mechanism, *via* single crystal X-ray diffraction, SEM, and photoluminescence spectroscopy, as well as theoretical calculations. Moreover, Schiff base **HNP** can act as a 'turn-off' fluorescence sensor for potential applications in Cu^{2+} detection.

2. Results and discussion

2.1 Synthesis

The synthetic route to Schiff base N^2,N^6-bis(2-(2-hydroxynaphthalen-1-yl)phenyl)pyridine-2,6-dicarboxamide (**HNP**) is presented in Scheme 1. The intermediate N,N'-(2-aminophenyl)-2,6-dicarboxylimide pyridine (**1**) was synthesized according to a previous report.[14] Treatment of **1** with 2-hydroxy-1-naphthaldehyde dissolved in methanol afforded the target red compound **HNP** in 78% yield. Interestingly, a yellow powder was obtained when more than 0.3 equivalents of H_2SO_4 catalyst was added to the reaction, which shows the same characterization data for the $^1H/^{13}C$ NMR spectroscopy (Fig. S1 and S2, ESI†) and high-resolution mass spectrometry (HRMS) (Fig. S3, ESI†) as compound **HNP**.

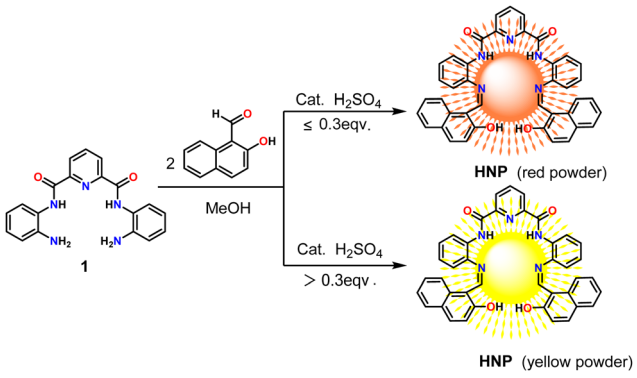

Scheme 1 Synthesis of compound **HNP**.

2.2 Photophysical properties

The UV-vis absorption spectra and photoluminescence (PL) spectra of compound **HNP** were measured in seven solutions (CH_3OH, EtOH, $CHCl_3$, THF, DCM, DMSO and DMF) and are shown in Fig. S4 (ESI†). The absorption band at λ = 319 nm represents the electronic transition of the Schiff base unit,[19] and the absorption peak at λ = 396 nm is tentatively assigned to the electron–electron transition from the Schiff base to the amide–pyridine ring, which is greatly affected by the polarity of the solvent.[20] Meanwhile, the wide absorption wavelength range from 419 nm to 475 nm is due to the formation of intramolecular hydrogen bonds.[21] In addition, the compound **HNP** exhibits weak fluorescence in all solvents, but the fluorescence intensity is stronger in weak polarity solvents (such as $CHCl_3$, THF and DCM) than in strong polarity solvents (CH_3OH, EtOH, DMF and DMSO). Moreover, the compound exhibits a red-shifted emission in the protic solvents methanol and ethanol as compared to DMSO, and this may be ascribed to the presence of the —OH group which can stabilize the enol conformation and lead to the adoption of a twisted intramolecular charge transfer (TICT) process.[22]

2.3 Aggregation-induced emission properties

To understand the effect of water on the emission process, the UV-vis spectra and photoluminescence (PL) spectra characteristics were studied in a mixture of THF/H_2O with different water fractions (f_w). As shown in Fig. S5, (ESI†) the peak at 419–475 nm gradually decreases, which may be attributed to the blocking of the ESIPT by the intermolecular H-bonding between the **HNP** and H_2O.[23] On the other hand, as shown in Fig. 1, a dual emission in THF was observed under excitation (λ_{ex} = 350 nm), the short-wavelength emission originating from enol emission and the latter from keto emission.[22] Moreover, the shorter-wavelength emission decreased gradually with the increase of water content, and eventually disappeared when the water fraction (f_w) increased to more than 80%. This is attributed to molecular aggregation, resulting in strengthened intramolecular H-bonding, which is a key factor for an efficient ESIPT process.[12] Furthermore, **HNP** emits weak orange emission with a maximum emission peak at 588 nm, as the water fraction (f_w) increased from 0% and 70%, and the emission intensity gradually decreased with the increase of water content. This is consistent with the UV-vis spectra, which show that the fluorescence intensity is reduced. As the water fraction (f_w) increased from 70% to 95%, the emission intensity was enhanced *ca.* 3.5-fold, indicating that **HNP** exhibits a clear aggregation-induced enhanced emission (AIEE). To further investigate the aggregation-induced emission (AIE) properties of **HNP**, the emission spectra were recorded with a different

Open Access Article. Published on 08 July 2022. Downloaded on 1/13/2026 10:55:49 PM.
This article is licensed under a Creative Commons Attribution 3.0 Unported Licence.

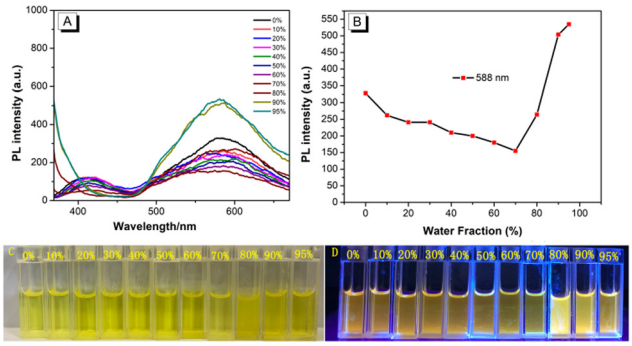

Fig. 1 (A) Fluorescence spectra of the fluorescent probe (2.00×10^{-5} mol L^{-1}) at different water contents (λ_{ex} = 350 nm) in THF. (B) The effect of water volume fraction on the fluorescence probe at 588 nm. (C) Photographs of the fluorescent probes in THF solution containing different water components under natural light. (D) Photographs of the fluorescent probes in THF solution containing different water components under 365 nm UV light.

excitation (λ_{ex} = 440 nm) and higher concentration (5.00×10^{-5} mol L^{-1}) in THF solution using different THF/water mixtures. The results revealed almost the same trend, where the overall fluorescence intensity was enhanced (Fig. S6, ESI†). Moreover, the stability of the probe **HNP** at various pH values was examined in the THF/water (V_{THF}/V_{water} = 1/9, Tris-HCl buffer) system (Fig. S7, ESI†). With the changing pH, the absorbance of **HNP** gradually decreases as the pH value increases from 1.00 to 3.00, while the absorbance exhibits a slight change over the pH range from 5.00 to 12.00. On the other hand, the fluorescence intensity remains unchanged in the pH range from 1.00 to 12.00. This result indicated that the Schiff-based compound **HNP** was stable at various pH values from 2.00 to 12.00.

2.4 Mechanochromism properties

As we know, most AIE luminogens exhibit excellent reversible mechanochromism properties under external stimulation. Considering the flexibility of the molecular structure of **HNP**, the reversible mechanochromism behaviour was studied. The yellow compound **HNP** displays a bright orange emission with a maximum emission peak at λ_{em} = 540 nm, (Φ_f = 5.44%). Once the yellow compound **HNP** was ground, the powder emitted a large, red-shifted emission with λ_{maxem} = 662 nm (Φ_f = 1.55%), and the fluorescence lifetime (τ) changed from 5.35 ns (**HNP-*y***) to 1.81 ns. Moreover, the red emission powder could recover the yellow emission under a CH_2Cl_2 atmosphere, indicating that **HNP** displays reversible mechanical stimuli-responsive properties. Furthermore, the samples of **HNP** before and after grinding were evaluated by powder X-ray diffraction. As shown in Fig. 2, the crystal sample **HNP-*y*** exhibits sharp intensity peaks, indicative of a good microcrystalline structure, while powdered **HNP-*r*** displays weak and broad diffraction peaks, and the peaks at 2θ = 12° and 16° almost disappeared after grinding, indicating that the molecular arrangement displays a large change with a red-shifted emission. Moreover, the diffraction peak of **HNP-*r*** can return back to a sharp peak *via* CH_2Cl_2

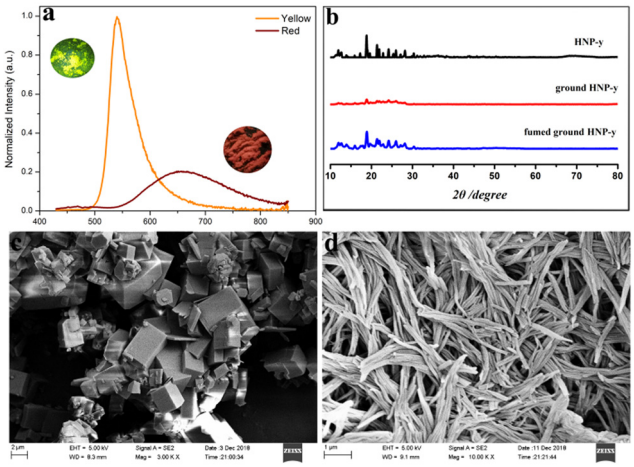

Fig. 2 (a) Fluorescence spectra of powdered **HNP-*y*** (orange line) and powdered **HNP-*r*** (red line). (b) PXRD patterns of crystals of **HNP-*y*** and **HNP-*r*** and when ground and after fuming with CH_2Cl_2. SEM image of **HNP** powder under different fluorescent emissions (c) yellow and (d) red.

fuming, and the emission colour changes from red to orange, and this process agrees with their optical behaviour. Additionally, the morphology of the samples **HNP-*y*** and **HNP-*r*** was also investigated by scanning electron microscopy (SEM). As shown in Fig. 2c, crystalline **HNP-*y*** exhibits a block 3D aggregate structure, while powdered **HNP-*r*** shows a 2D fibrous-like structure along the same direction (Fig. 2d), indicating that **HNP** show different morphology before and after grinding, which was further characterized by the UV-Vis absorption spectra and is illustrated in Fig. S8 (ESI†). After fuming with CH_2Cl_2, the UV-vis absorption of the samples is almost overlapped with the crystalline **HNP-*y***.

2.5 Single crystal structure analysis

Single crystal X-ray diffraction is an efficient tool to visualize the molecular conformation and for understanding the relationship between the molecular packing and the optical behaviour. Thus, we attempted to cultivate crystals of **HNP** by slow solvent evaporation at room temperature. Firstly, pure **HNP** (20 mg) was dissolved in a chloroform/ethanol mixture to obtain block red crystals (**HNP-*r***); yield 12 mg. Then, the mother liquor was collected to afford yellow needle crystals (**HNP-*y***) (yield 6 mg). Both molecular structures of the crystals **HNP-*y*** and **HNP-*r*** were confirmed by single crystal X-ray diffraction analysis, and the key crystal data are summarized in Table S1 (ESI†). The **HNP-*y*** crystal belongs to the triclinic crystal system with the space group $P\bar{1}$, and the asymmetric unit cell of **HNP-*y*** contains two molecules. Meanwhile, the crystal **HNP-*r*** crystallises in the higher symmetrical monoclinic system with the $C2/c$ space group, and each asymmetric unit contains four molecules. The ORTEP diagrams of **HNP-*y*** and **HNP-*r*** are shown in Fig. S9 (ESI†).

As shown in Fig. 3, the two terminal naphthyl rings in the crystal **HNP-*y*** adopt an intersecting type conformation, whereas the situation observed in **HMP-*r*** is almost coplanar.

Open Access Article. Published on 08 July 2022. Downloaded on 1/13/2026 10:55:49 PM.
This article is licensed under a Creative Commons Attribution 3.0 Unported Licence.

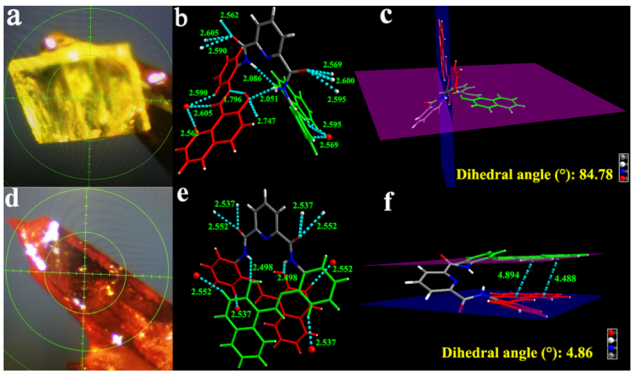

Fig. 3 (a) Photographs of **HNP-*y***. (b) Hydrogen bonding in **HNP-*y***. (c) Dihedral angle of the **HNP-*y*** crystal. (d) Photographs of **HNP-*r***. (e) Hydrogen bonding in **HNP-*r***. (f) Dihedral angle of the **HNP-*r*** crystal.

The difference is that one side of the planar group is almost perpendicular to another side plane with a dihedral angle of 84.78° in crystal **HNP-*y***. Two pairs of intramolecular hydrogen bond interactions (O2–H2B···N3 and O4–H4B···N5) are formed between the hydroxyl and imino groups at distances of 1.776 Å and 1.794 Å, respectively, which are shorter than our previous reported tetraphenylethylene functionalised salicylaldehyde Schiff-base (1.882 Å and 1.858 Å),[14] and other intramolecular hydrogen bonds (N–H···O and N–H···O), *e.g.* 2.051 Å and 2.086 Å, respectively,[16] which indicated that the intramolecular hydrogen bond is stronger here. For crystal **HNP-*r***, the two planar groups are almost parallel, and the dihedral angle is 4.86°, and the the distance between the centres of the terminal naphthyl rings is in the range 4.488–4.894 Å, suggesting that **HNP-*r*** prefers to form π–π stacking. Also, intramolecular hydrogen bonding (O–H···N) is observed at a distance of 1.822 Å. The intramolecular hydrogen bonds (N2–H2A···O2′) are both 2.498 Å long.

In the packing of the structure, the **HNP-*y*** molecules are connected by intermolecular π–π interactions and multiple C–H···O hydrogen bonds between adjacent molecules. Furthermore, intermolecular π···π interactions are observed between two naphthyl rings and two adjacent molecules at a distance of 3.35 Å and 3.36 Å. Multiple intermolecular bonds C–H···O interactions were formed between the carbonyl oxygen atoms with the phenyl ring or the naphthyl ring of the adjacent molecules. These intermolecular forces enable the **HNP-*y*** molecules to adopt a parallel arrangement forming columns overlapping along the *a*-axis (Fig. 4a), and the adjacent molecules in the adjacent columns overlap with each other with anti-parallel π-overlap (Fig. 4b).

On the other hand, for the **HNP-*r*** crystals, the adjacent molecules are connected by π···π stacking between the phenyl and pyridine rings (≈ 3.38 Å), thereby forming a three-dimensional structure (Fig. 4c). Each of the adjacent molecules are arranged in an anti-parallel direction along the *c*-axis (Fig. 4d). Infinite stacking was also observed in each column, but compared with **HNP-*y*** crystals, intermolecular overlap was smaller and the arrangement was less orderly.

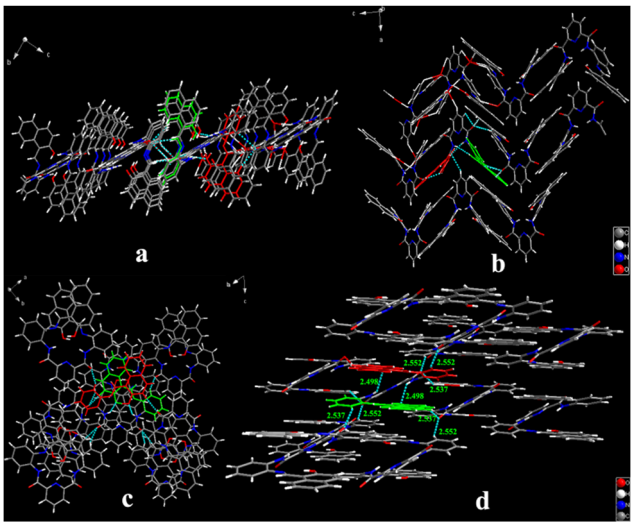

Fig. 4 (a) Molecular packing structures, intermolecular interactions in the ordered structure of the **HNP-*y*** crystal. (b) Two adjacent dimers and intermolecular interactions of the **HNP-*y*** crystal. (c) Molecular packing structures, intermolecular interactions in the ordered structure of the **HNP-*r*** crystal. (d) Two adjacent dimers and intermolecular interactions of the **HNP-*r*** crystal. The blue dotted lines indicate intermolecular interactions.

Moreover, the simulated X-ray diffraction (XRD) patterns of **HNP-*y*** and **HNP-*r*** crystals totally coincided with that of **HNP-*y*** and **HNP-*r*** crystalline powders, respectively, suggesting the same molecular packing modes in them. However, compared to the powder X-ray diffraction data, the **HNP-*y*** crystals and **HNP-*r*** crystals show different diffraction peaks, indicated that both crystals **HNP-*y*** and **HNP-*r*** arrange in different stacking modes (Fig. S10, ESI†). Indeed, the crystals **HNP-*y*** and **HNP-*r*** emit a yellow and red emission with maximum emission peak at 540 nm and 662 nm, respectively. This result is also consistent with the mechanochromism behaviour.

2.6 Theoretical calculations

In order to explore the electronic structures of the **HNP-y** and **HNP-r** molecules, density functional theory (DFT) and time-dependent DFT (TD-DFT) calculations were performed using the B3LYP/6-31G(d) basis set. As shown in Fig. 5, the HOMO and LUMO levels of **HNP-*y*** are almost spread over the whole molecular framework, while the HOMO level of **HNP-*r*** is mainly localized on the phenyl and naphthyl parts, while the LUMO level is distributed on the naphthyl fragments. Moreover, the energy gap (E_g) of **HNP-*r*** (3.59 eV) is higher than **HNP-*r*** (3.44 eV). TD-DFT calculations indicating that the main absorption for **HNP-*r*** is assigned to the S_1–S_0 transition from HOMO to LUMO, in which the HOMO → LUMO contribution in **HNP-*r*** is 91.1%, and the HOMO → LUMO contribution in **HNP-*y*** is only 60.0%.[24] Thus, the molecular conformation has a significant influence on the excited state properties and on the oscillator strength (f) of the S_1–S_0 transition.[22] Based on the results of the calculations and the molecular structure, the dihedral angle of the two naphthyl groups decreases, and

Open Access Article. Published on 08 July 2022. Downloaded on 1/13/2026 10:55:49 PM.
This article is licensed under a Creative Commons Attribution 3.0 Unported Licence.

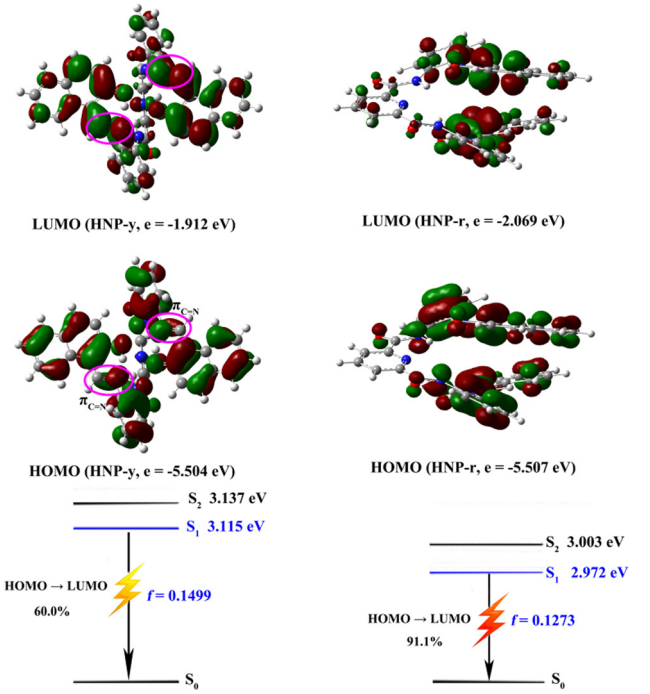

Fig. 5 The frontier orbitals and theoretically calculated vertical excitation energies, transition natures of the excited states and oscillator strengths for **HNP-*y*** and **HNP-*r***.

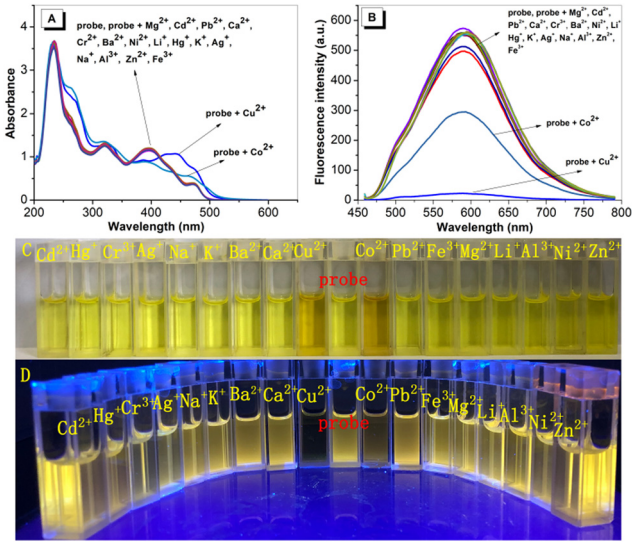

Fig. 6 (A) UV-vis absorption spectra and (B) fluorescence spectra of fluorescent probes (5.00×10^{-5} mol L^{-1}) interacting with different metal ions (1.00×10^{-4} mol L^{-1}) in THF solution (λ_{ex} = 440 nm); (C) photographs of the probes interacting with metal ions under natural light; (D) photographs of the probes interacting with metal ions under 365 nm UV illumination.

the f value reduces from 0.1499 to 0.1273, suggesting that a decreased twist of the dihedral angle results in a red-shifted emission with weaker emission. Therefore, it would be a useful strategy to change the ability of the electron donor or electron acceptor to regulate the charge transfer efficiency in order to achieve a high fluorescence yield in this type of luminescence material.

2.7 Fluorogenic Cu^{2+} sensing

In order to evaluate the sensing properties of **HNP**, its sensing properties in THF with several metal cations (solutions of Hg^{+}, Cr^{3+} and Mg^{2+} and Zn^{2+} were prepared from their chloride salts; solutions of Cu^{2+}, Cd^{2+}, Pb^{2+}, Ca^{2+}, Co^{2+}, Ba^{2+}, Ag^{+}, Ni^{2+}, Li^{+}, K^{+}, Na^{+}, Al^{3+}, Zn^{2+} and Fe^{3+} were prepared from their nitrate salts) were investigated by UV-vis absorption and fluorescence measurements (Fig. 6). The absorption spectra of **HNP** showed that the absorption peak at 396 nm remained unchanged upon addition of several kinds of metal ions except in the case of Cu^{2+} and Co^{2+}. Upon addition of Cu^{2+}, the absorbance located at 396 nm was red shifted to 443 nm. Except for Co^{2+}, other metal ions had little effect on the absorption. The fluorescence emission at 588 nm upon excitation by 440 nm was quenched upon addition of Cu^{2+}, while other metal cations had little effect on the fluorescence intensity of the probe. Moreover, competition experiments were conducted, and as shown in Fig. S11 (ESI†), other metal ions did not interfere with the recognition of **HNP** toward Cu^{2+}, with the exception of Co^{2+} which had a slight effect on the probe detection of Cu^{2+}, indicating that the probe had strong anti-interference properties. The results of UV-Vis absorption spectra and fluorescence spectra show that the probe has high specificity toward copper ions. Moreover, fluorescence titration experiments of Cu^{2+} were carried out in THF. As shown in Fig. S12 (ESI†), the absorbance of the probe at 396 nm gradually decreased with the increase of Cu^{2+} concentration; meanwhile, a new absorbance at 443 nm gradually increased. Moreover, the fluorescence intensity of the probe decreased gradually at 588 nm, and the fluorescence quenching rate reached 95.35% when two equivalents of Cu^{2+} were added. Additionally, the combination ratio between them was further determined by the equal mole continuous transformation method (Job's plot). As shown in Fig. S13 (ESI†), through the fluorescence spectrum, it can be seen that probe/probe + Cu^{2+} has an inflection point at 0.33, indicating that the mixing ratio between probe and Cu^{2+} is 1 : 2.

Furthermore, the detection limit of probe **HNP** for Cu^{2+} was calculated to be 1.8×10^{-7} mol L^{-1} from the fluorescence titration experiments following the IUPAC method (Fig. S14, ESI†).[25] On the basis of the 2 : 1 stoichiometry, the association constant between **HNP** and Cu^{2+} was estimated to be 5.70×10^{3} mol L^{-1} by using the Benesi–Hildebrand equation (Fig. S15, ESI†).[26]

The crystal structure is important for us to understand the coordination mode and molecular packing. Fortunately, single crystals of complex **HNP-Cu** were obtained by slow evaporation from solutions in ethanol at room temperature. The crystal data are summarized in Table S1 (ESI†). The complex **HNP-Cu** crystallizes in the orthorhombic system and each unit cell contains two complex molecules. Moreover, as shown in Fig. S16a (ESI†), one **HNP** molecule coordinates with two Cu^{2+} ions, which is consistent with the titration experiments. Each Cu atom is four-coordinate with four atoms (oxygen and

Open Access Article. Published on 08 July 2022. Downloaded on 1/13/2026 10:55:49 PM. This article is licensed under a Creative Commons Attribution 3.0 Unported Licence.

nitrogen atoms), which results in removal of the hydrogen ions of the hydroxyl groups and thus the process of ESIPT was intercepted, so that it shows fluorescence quenching. The two planes of the terminal aromatic rings of **HNP** are parallel; therefore, a 1D chain was formed by countless helices in the same direction *via* intermolecular π···π interactions ($d \approx 3.30$ Å) and intramolecular hydrogen bond interactions (Fig. S16b, ESI†). **HNP** is a highly selective and sensitive chemosensor for Cu^{2+} ions.

3. Conclusions

In summary, we report here a naphthaldehyde based Schiff base material with both excited state intramolecular proton transfer and AIEgen fluorescence emission which can undergo a polymorphic switch on changing the solvent. Crystals of both **HNP-*y*** and **HNP-*r***, with different emission colours were obtained by slow evaporation in chloroform/ethanol mixtures. Single crystal X-ray diffraction data and DFT calculations show that the **HNP-*r*** molecule is formed in a more compact stacking mode due to the smaller dihedral angle of the terminal aromatic ring planes and stronger intermolecular interactions, resulting in a red-shifted emission and weaker fluorescence emission. The multiple stimuli-responsive behaviour of **HNP** results in mechanochromic luminescence and its ability to act as a sensitive chemosensor for the Cu^{2+} ion. Our work provides a strategy for further understanding the relationship between the molecular structure and the emission mechanism at the molecular level and for the design of multi-stimuli responsive materials and can contribute to the understanding and the future design of new mechanochromic luminescent materials. It will stimulate a new approach for the realization of mechanochromic luminescent materials and provide a new understanding of the nature of mechanochromic behaviour.

Author contributions

Lingyi Shen carried out the experiments, wrote the paper and analyzed the X-ray structure. Chang-Jin Yu, carried out the experiments and wrote the paper. Hai-Fang Xie and Na Xu carried out the experiments. Hong Xu analyzed the experimental data. Ya-Li Huang provided experimental guidance. Xing Feng provided experimental guidance and design. Carl Redshaw analyzed the experimental data and revised the paper. Qi-Long Zhang provided research ideas, designed the experiments and modified the paper.

Conflicts of interest

There are no conflicts to declare.

Acknowledgements

This work was supported by the National Natural Science Foundation of China (22065009 and 22066007), Guizhou Provincial Natural Science Foundation ZK[2021]076, Guizhou Provincial Department of Education Foundation KY[2022]229 and the Guizhou Province College Students Innovation and Entrepreneurship Project (S202110660004). C. R. thanks the EPSRC for an Overseas Travel Grant (EP/R23816/1).

Notes and references

1 (*a*) S. Mo, Q. Meng, S. Wan, Z. Su, H. Yan, B. Z. Tang and M. Yin, Tunable mechanoresponsive self-assembly of an amide-linked dyad with dual sensitivity of photochromism and mechanochromism, *Adv. Funct. Mater.*, 2017, **27**, 1701210; (*b*) W. Li, Q. Huang, Z. Mao, Q. Li, L. Jiang, Z. Xie, R. Xu, Z. Yang, J. Zhao, T. Yu, Y. Zhang, M. P. Aldred and Z. Chi, Alkylchain introduction: *in situ* solar-renewable colorful organic mechanoluminescence materials, *Angew. Chem., Int. Ed.*, 2018, **57**, 12727–12732; (*c*) Y. Li, S. Liu, T. Han, H. Zhang, C. Chuah, R. T. K. Kwok, J. W. Y. Lam and B. Z. Tang, Sparks fly when AIE meets with polymers, *Mater. Chem. Front.*, 2019, **3**, 2207–2220; (*d*) M. A. C. Stuart, W. T. S. Huck, J. Genzer, M. Müller, C. Ober, M. Stamm, G. B. Sukhorukov, I. Szleifer, V. V. Tsukruk, M. Urban, F. Winnik, S. Zauscher, I. Luzinov and S. Minko, Emerging applications of stimuli-responsive polymer materials, *Nat. Mater.*, 2010, **9**, 101–113; (*e*) Y. Sagara, S. Yamane, M. Mitani, C. Weder and T. Kato, Mechanoresponsive luminescent molecular assemblies: an emerging class of materials, *Adv. Mater.*, 2016, **28**, 1073–1095.

2 (*a*) Z. Yang, Z. Chi, Z. Mao, Y. Zhang, S. Liu, J. Zhao, M. P. Aldred and Z. Chi, Recent advances in mechanoresponsive luminescence of tetraphenylethylene derivatives with aggregation-induced emission properties, *Mater. Chem. Front.*, 2018, **2**, 861–890; (*b*) L. Tan, S. Mo, B. Fang, W. Cheng and M. Yin, Dual fluorescence switching of a Rhodamine 6G-naphthalimide conjugate with high contrast in the solid state, *J. Mater. Chem. C*, 2018, **6**, 10270–10275.

3 (*a*) X. Guo, D. Zhang and D. Zhu, Logic control of the fluorescence of a new dyad, spiropyran-perylene diimide-spiropyran, with light, ferric ion, and proton: construction of a new three-input "AND" logic gate, *Adv. Mater.*, 2004, **16**, 125–130; (*b*) F. M. Raymo, R. J. Alvarado, S. Giordani and M. A. Cejas, Memory effects based on intermolecular photo-induced proton transfer, *J. Am. Chem. Soc.*, 2003, **125**, 2361–2364; (*c*) L. Zhu, M.-Q. Zhu, J. K. Hurst and A. D. Q. Li, Light-controlled molecular switches modulate nanocrystal fluorescence, *J. Am. Chem. Soc.*, 2005, **127**, 8968–8970.

4 Z. Wang, F. Yu, W. Chen, J. Wang, J. Liu, C. Yao, J. Zhao, H. Dong, W. Hu and Q. Zhang, Rational control of charge transfer excitons toward high-contrast reversible mechanoresponsive luminescent switching, *Angew. Chem., Int. Ed.*, 2020, **59**, 17580–17586.

5 (*a*) G. Huang, Y. Jiang, S. Yang, B. S. Li and B. Z. Tang, Multistimuli response and polymorphism of a novel tetraphenylethylene derivative, *Adv. Funct. Mater.*, 2019, **29**, 1900516; (*b*) Z. Lu, S. Yang, X. Liu, Y. Qin, S. Lu,

Open Access Article. Published on 08 July 2022. Downloaded on 1/13/2026 10:55:49 PM. This article is licensed under a Creative Commons Attribution 3.0 Unported Licence.

Y. Liu, R. Zhao, L. Zheng and H. Zhang, Facile synthesis and separation of *E*/*Z* isomers of aromatic-substituted tetraphenylethylene for investigating their fluorescent properties via single crystal analysis, *J. Mater. Chem. C*, 2019, **7**, 4155–4163.

6 (*a*) X. Feng, J. Zhang, Z. Hu, Q. Wang, M. M. Islam, J.-S. Ni, M. R. J. Elsegood, J. W. Y. Lam, E. Zhou and B. Z. Tang, Pyrene-based aggregation-induced emission luminogens (AIEgen): structure correlated with particle size distribution and mechanochromism, *J. Mater. Chem. C*, 2019, **7**, 6932–6940; (*b*) J. Zeng, X. Wang, X. Song, Y. Liu, B. Liao, J. Bai, C. Redshaw, Q. Chen and X. Feng, Steric influences on the photophysical properties of pyrene-based derivatives; mechanochromism and their pH-responsive ability, *Dyes Pigm.*, 2022, **200**, 110123.

7 B. Huang, Z. Li, H. Yang, D. Hu, W. Wu, Y. Feng, Y. Sun, B. Lin and W. Jiang, Bicolour electroluminescence of 2-(carbazol-9-yl)anthraquinone based on a solution process, *J. Mater. Chem. C*, 2017, **5**, 12031–12034.

8 (*a*) J. Luo, Z. Xie, J. W. Y. Lam, L. Cheng, H. Chen, C. Qiu, H. S. Kwok, X. Zhan, Y. Liu, D. Zhu and B. Z. Tang, Aggregation-induced emission of 1-methyl-1,2,3,4,5-pentaphenylsilole, *Chem. Commun.*, 2001, 1740–1741; (*b*) Y. Hong, J. W. Y. Lam and B. Z. Tang, Aggregation-induced emission, *Chem. Soc. Rev.*, 2011, **40**, 5361–5388; (*c*) J. Huang, N. Sun, J. Yang, R. Tang, Q. Li, D. Ma and Z. Li, Blue aggregation induced emission luminogens: high external quantum efficiencies up to 3.99% in LED device, and restriction of the conjugation length through rational molecular design, *Adv. Funct. Mater.*, 2014, **24**, 7645–7654; (*d*) H. Wu, X.-C. Fan, H. Wang, F. Huang, X. Xiong, Y.-Z. Shi, K. Wang, J. Yu and X.-H. Zhang, Conformational isomerization: A novel mechanism to realize the AIE-TADF behaviors, *Aggregate*, 2022, DOI: **10.1002/agt2.243**.

9 (*a*) V. S. Padalkar and S. Seki, Excited-state intramolecular proton-transfer (ESIPT)-inspired solid state emitters, *Chem. Soc. Rev.*, 2016, **45**, 169–202; (*b*) G. Yang, Y. Ran, Y. Wu, M. Chen, Z. Bin and J. You, Endowing imidazole derivatives with thermally activated delayed fluorescence and aggregation-induced emission properties for highly efficient non-doped organic light-emitting diodes, *Aggregate*, 2021, **3**, e127, DOI: **10.1002/agt2.127**; (*c*) T. Zhou, T. Jia, B. Kang, F. Li, M. Fahlman and Y. Wang, Nitrile-substituted QA derivatives: new acceptor materials for solution-processable organic bulk heterojunction solar cells, *Adv. Energy Mater.*, 2011, **1**, 431–439; (*d*) C. Wang, K. Wang, Q. Fu, J. Zhang, D. Ma and Y. Wang, Pentaphenylphenyl substituted quinacridone exhibiting intensive emission in both solution and solid state, *J. Mater. Chem. C*, 2013, **1**, 410–413.

10 Y. Li, R. Zhang, Q. Wan, R. Hu, Y. Ma, Z. Wang, J. Hou, W. Zhang and B. Z. Tang, Trojan horse-like nano-AIE aggregates based on homologous targeting strategy and their photodynamic therapy in anticancer application, *Adv. Sci.*, 2021, **8**, 2102561.

11 (*a*) J. Zhao, S. Ji, Y. Chen, H. Guo and P. Yang, Excited state intramolecular proton transfer (ESIPT): from principal photophysics to the development of new chromophores and applications in fluorescent molecular probes and luminescent materials, *Chem. Chem. Phys.*, 2012, **14**, 8803–8817; (*b*) M. K. Bera, C. Chakraborty, P. K. Singh, C. Sahu, K. Sen, S. Maji, A. K. Das and S. Malik, Fluorene-based chemodosimeter for "turn-on" sensing of cyanide by hampering ESIPT and live cell imaging, *J. Mater. Chem. B*, 2014, **2**, 4733–4739.

12 (*a*) K. Sakai, T. Ishikawa and T. Akutagawa, A blue-white-yellow color-tunable excited state intramolecular proton transfer (ESIPT) fluorophore: sensitivity to polar–nonpolar solvent ratios, *J. Mater. Chem. C*, 2013, **1**, 7866–7871; (*b*) Y. Hong, J. W. Y. Lam and B. Z. Tang, Aggregation-induced emission, *Chem. Soc. Rev.*, 2011, **40**, 5361.

13 Z. Hu, H. Zhang, Y. Chen, Q. Wang, M. R. J. Elsegood, S. J. Teat, X. Feng, M. M. Islam, F. Wu and B. Z. Tang, Tetraphenylethylene-based color-tunable AIE-ESIPT chromophores, *Dyes Pigm.*, 2020, **175**, 108175.

14 H.-F. Xie, C.-J. Yu, Y.-L. Huang, H. Xu, Q.-L. Zhang, X.-H. Sun, X. Feng and C. Redshaw, A turn-off fluorescent probe for the detection of Cu^{2+} based on a tetraphenylethylene-functionalized salicylaldehyde Schiff-base, *Mater. Chem. Front.*, 2020, **4**, 1500–1506.

15 C. Redshaw, M. R. J. Elsegood, J. W. A. Frese, S. Ashby, Y. Chao and A. Mueller, Cellular uptake studies of two hexanuclear, carboxylate bridged, Zinc ring structures using fluorescence microscopy, *Chem. Commun.*, 2012, **48**, 6627–6629.

16 X. Zhang, S.-T. Wu, X.-J. Yang, L.-Y. Shen, Y.-L. Huang, H. Xu, Q.-L. Zhang, T. Sun, C. Redshaw and X. Feng, Dynamic Coordination between a Triphenylamine-Functionalized Salicylaldehyde Schiff Base and a Copper(II) Ion, *Inorg. Chem.*, 2021, **60**, 8581–8591.

17 (*a*) F. Han, R. Zhang, Z. Zhang, J. Sua and Z. Ni, A new TICT and AIE-active tetraphenylethene-based Schiff base with reversible piezofluorochromism, *RSC Adv.*, 2016, **6**, 68178–68184; (*b*) P. Yadav, A. K. Singh, C. Upadhyay and V. P. Singh, Photoluminescence behaviour of a stimuli responsive Schiff base: Aggregation induced emission and piezochromism, *Dyes Pigm.*, 2019, **160**, 731–739; (*c*) I. Majumder, P. Chakraborty, S. Dasgupta, C. Massera, D. Escudero and D. Das, A Deep Insight into the photoluminescence properties of Schiff base Cd^{II} and Zn^{II} complexes, *Inorg. Chem.*, 2017, **56**, 12893–12901.

18 Y. Nie, H. Zhang, J. Miao, X. Zhao, Y. Li and G. Sun, Synthesis, aggregation-induced emission and mechanochromism of a new carborane-tetraphenylethylene hybrid, *J. Organomet. Chem.*, 2018, **865**, 200–205.

19 (*a*) A. Klein, A.-K. Schmieder, N. Hurkes, C. Hamacher, A. O. Schüren, M. P. Feth and H. Bertagnolli, Mono- and Binuclear Arylnickel Complexes of the α-Diimine Bridging Ligand 2,2′-Bipyrimidine (bpym), *Eur. J. Inorg. Chem.*, 2010, 934–941; (*b*) L. Shen, Y. Zhao, Q. Luo, Q.-S. Li, B. Liu, C. Redshaw, B. Wu and X.-J. Yang, Cyclotrimerization of alkynes catalyzed by a self-supported cyclic tri-nuclear nickel(0) complex with α-diimine ligands, *Dalton Trans.*, 2019, **48**, 4643.

20 (*a*) E. Ragnoni, D. M. Di, A. Iagatti, A. Lapini and R. Righini, Mechanism of the intramolecular iharge transfer state formation in all-trans-β-Apo-8′-carotenal: influence of solvent

Open Access Article. Published on 08 July 2022. Downloaded on 1/13/2026 10:55:49 PM.
This article is licensed under a Creative Commons Attribution 3.0 Unported Licence.

polarity and polarizability, *J. Phys. Chem. B*, 2015, **119**, 420–432; (*b*) Y. J. Zhang, K. Wang, G. L. Zhuang, Z. Q. Xie, C. Zhang, F. Cao, G. X. Pan, H. F. Chen, B. Zou and Y. G. Ma, Multicolored-fluorescence switching of ICT-type organic solids with clear color difference: mechanically controlled excited state, *Chem. – Eur. J.*, 2015, **21**, 2474–2479; (*c*) V. A. Galievsky, S. I. Druzhinin, A. Demeter, P. Mayer, S. A. Kovalenko, T. A. Senyushkina and K. A. Zachariasse, Ultrafast intramolecular charge transfer with *N*-(4-cyanophenyl)carbazole. evidence for a LE precursor and dual LE + ICT fluorescence, *J. Phys. Chem. A*, 2010, **114**, 12622–12638.

21 Q. Yu, X. Zhang, S.-T. Wu, H. Chen, Q.-L. Zhang, H. Xu, Y.-L. Huang, B.-X. Zhu and X.-L. Ni, Twisted Schiff-base macrocycle showing excited-state intramolecular proton-transfer (ESIPT): assembly and sensing properties, *Chem. Commun.*, 2020, **56**, 2304–2307.

22 M. Das, M. Brahma and G. Krishnamoorthy, Light-driven switching between intramolecular proton-transfer and charge-transfer states, *J. Phys. Chem. B*, 2021, **125**, 2339–2350.

23 J. E. Kwon and S. Y. Park, Advanced organic optoelectronic materials: Harnessing excited-state intramolecular proton transfer (ESIPT) process, *Adv. Mater.*, 2011, **23**, 3615–3642.

24 H.-W. Zheng, S. Li, M. Wu, Y. Kang, J.-B. Li, Q.-F. Liang, X.-J. Zheng, D.-C. Fang and L.-P. Jin, Multi-stimuli responsive behaviors of two TPE-based tautomers in the solid state and in solution, *J. Mater. Chem. C*, 2020, **8**, 4246–4252.

25 G. L. Long and J. D. Winefordner, Limit of detection. A closer look at the IUPAC definition, *Anal. Chem.*, 1983, **55**, 712A–724A.

26 P. Thordarson, Determining association constants from titration experiments in supramolecular chemistry, *Chem. Soc. Rev.*, 2011, **40**, 1305–1323.